Journal of South American Earth Sciences 98 (2020) 102435

Contents lists available at ScienceDirect

Journal of South American Earth Sciences

journal homepage: www.elsevier.com/locate/jsames

Genesis and variation spatial of Podzol in depressions of the Barreiras Formation, northeastern Espírito Santo State, Brazil, and its implications for Quaternary climate change

Jolimar Antonio Schiavo[a,*], Luiz Carlos Ruiz Pessenda[b], Antonio Alvaro Buso Júnior[b], Marcia Regina Calegari[c], Mileni Fornari[b], Mateus Luiz Secretti[a], Marcos Gervasio Pereira[d], Francis Edward Mayle[e]

[a] Universidade Estadual de Mato Grosso do Sul, Unidade Universitária de Aquidauana, Rodovia Aquidauana, km 12, Aquidauana, Mato Grosso do Sul, Brazil
[b] Universidade de São Paulo, Laboratório de ^{14}C, Avenida Centenário 303, 13400-970, Piracicaba, São Paulo, Brazil
[c] Universidade Estadual do Oeste do Paraná, Campus Marechal Cândido Rondon, Colegiado de Geografia, Rua Pernambuco, 1777, CX Postal 91, CEP:85970-020, Mal. Cd Rondon, Paraná, Brazil
[d] Universidade Federal Rural do Rio de Janeiro, Instituto de Agronomia, Departamento de Solos, BR-465, Seropédica, Rio de Janeiro, Brazil
[e] University of Reading, Centre for Past Climate Change and Department of Geography & Environmental Science, Reading RG6 6DW, Berkshire, UK

ARTICLE INFO

Keywords:
Ground penetrating radar
Organic matter
Stable carbon isotopes
^{14}C dating
Micromorphology
Podzolisation

ABSTRACT

Variations in relief associated with pedogenetic processes promote different intensities in weathering of sediments of the Barreiras Formation and may thus lead to the formation of different soil types, like Podzols, Acrisols and Ferralsols. The Podzols of tropical regions contain important information on climate and vegetation changes that occurred mainly in late Pleistocene and Holocene; however few studied, regarding their spatial variation, that can be investigated through ground penetrating radar (GPR). The aim was to study morphological, physical, chemical, stable C isotopic properties and spatial distribution of soils within depressions of the Barreiras Formation and characterize the ^{14}C chronology of two Podzols and their B spodic horizons, along a transect grassland to forest in northeastern Espírito Santo State, Brazil. The profiles encompass a sequence of A-E-Bhm horizons, except for P3 and P6 with histic H and A-Bt, respectively. The GPR images showed patterns corresponding to these soil horizons, and the GPR data reveal the presence of diagnostic subsurface horizons characteristic of spodic horizons with cemented layers. The influence of relief factors and original materials was observed, associated with ferrolysis and podzolisation as main actors in the genesis of soils studied. The monomorphic organic matter filling the voids evidences the processes of immobilization, illuviation and precipitation, with the genesis of the spodic horizon. The Podzols profiles of Pleistocene organic matter ages accumulated compounds of C_3 plants from the vegetation cover in the B spodic horizons of the profiles P4 and P1, since at least 14,251 and 38,890 cal BP, respectively, suggesting the dominance of a humid climate at least during the studied period in the region.

1. Introduction

The north and northeastern regions of Espírito Santo State, Brazil, encompass the Tabuleiros Costeiros (coastal plains) geomorphological unit, which comprises sandy-clayey Tertiary deposits of the Barreiras Group. In this coastal plain, there are gentle depressions, which favor the lateral flow of water with installation of water table, forming types of soils different from those of the higher parts of the landscape (Pessenda et al., 2015; Calegari et al., 2017).

Ferralsols and Acrisols are predominant soils and occupy the highest parts of the landscape of this region and have been well studied (Moreau et al., 2006; Corrêa et al., 2008; Lima Neto et al., 2009; Dantas et al., 2014), and are characterized by sandy loam to clay texture, yellowish tones, low nutrient availability and cation exchange capacity, exchangeable aluminum and aluminum saturation, and kaolinite mineralogy (Lima Neto et al., 2009). The lower parts of the landscape are associated with sandy soils like Arenosols and Podzols. In the coastal plains, the vegetation shows different physiognomies associated with markedly different soil types, i.e., Ferralsols and Acrisols are associated with Lowland Tropical Rainforest, while the Arenosols and Podzols are

* Corresponding author.
E-mail address: schiavo@uems.br (J.A. Schiavo).

https://doi.org/10.1016/j.jsames.2019.102435
Received 12 August 2019; Received in revised form 20 November 2019; Accepted 20 November 2019
Available online 23 November 2019

associated with the grasslands (Saporetti-Junior et al., 2012).

The Podzols have important environmental functions such as being a filter for pollutants and a sink for atmospheric carbon (Sauer et al., 2007; Montes et al., 2011; Lopes-Mazzetto et al., 2018), as well as representing areas with large numbers of endemic and niches specific species being designated as conservation areas (Buso Júnior et al., 2013; Mendonça et al., 2015).

Among the various theories proposed to explain the formation of Podzols (Anderson et al., 1982; Buurman and Jongmans, 2005; De Coninck, 1980; Lundstrom et al., 2000), the complexation and transport of dissolved organic matter (DOM) with Fe and Al play an important role in the formation of the B spodic horizon. Typically, the B spodic horizon shows colors ranging from black to reddish brown, enriched by organic matter, Al and sometimes Fe.

The natural drainage conditions influence the formation of Podzols, mainly in the morphology and distinction of horizons, in the accumulation and stabilization of organic matter and Fe in the B spodic horizon. The presence or absence of Fe can be used as an indicator of drainage conditions. Poorly drained Podzols have lost all Fe due to reduction and lateral removal, while in well-drained podzols Fe is still present, and intermediate drainage conditions are recognised by Fe mottles (Buurman, 1984; De Coninck et al., 1974). In addition to Fe, drainage conditions can cause variations in the morphology of Podzols as thickness of the B horizon and the shape of the EB transition, i.e. those poorly drained have flat EB transition caused by the highest groundwater level; while the well-drained have a thin undulating Bh horizon, dependent on the vertical movement of percolated water (Buurman et al., 2005, 2013; Lopes-Mazzetto et al., 2018; Kaczorek et al., 2004; Schwartz, 1988). In poorly drained podzols, the B horizon is water-saturated during large part of the year, and the organic matter is predominantly DOM derived. In well-drained podzols, the B horizon may have a contribution from in situ root materials and the DOM has a very local source due to vertical movement of percolating water (Lopes-Mazzetto et al., 2018). More detailed studies of organic matter such as determination of the elemental composition by pyrolysis (Lopes-Mazzetto et al., 2018), 12C and 13C isotopic variation, 14C dating (Horbe et al., 2004) and Spodic B horizon micromorphology (Bardy et al., 2008; Coelho et al., 2012) may contribute to inferring the genesis of Podzols.

The podzols of tropical environments, such as those of coastal plain in Brazil, may be much older and consequently with greater variations of climate and vegetation (Boski et al., 2015; Martinez et al., 2018), when compared to Podzols of boreal and temperate areas with Holocene age with moderate variations in the climate.

In Brazil, detailed studies of the classification and genesis of Podzols have been made in individual profiles (Mafra et al., 2002; Coelho et al., 2010; Coelho et al., 2010c; Oliveira et al., 2010; Schiavo et al., 2012; Carvalho et al., 2013), but little is known about the spatial variation of the podzolisation process as a function of climate and vegetation.

Vale Nature Reserve (VNR) is a 28,000-ha area of protected vegetation, located in the northeastern Espirito Santo State, in the municipality of Linhares, Brazil. The vegetation shows different physiognomies associated with markedly different soil types. Soil variations across the landscape can be better understood in the context of microrelief and associated variations in vegetation type. The Tabuleiros forest (Lowland Tropical Rainforest) is the dominant matrix, occurring in the higher parts of the landscape, being associated with Ferralsols and Acrisols (Moreau et al., 2006; Corrêa et al., 2008; Lima Neto et al., 2009; Silva et al., 2013; Dantas et al., 2014). Mussununga vegetation occurs interspersed with the Tabuleiros forest and varies from grasslands (campos nativos) to wooded savannah and woodland (Saporetti-Junior et al., 2012) and it is associated with sandy soils such as Arenosols and Podzols (Pessenda et al., 2015; Calegari et al., 2017; Buso Junior et al., 2019). In this region, these authors verified using distinct proxies (pollen, δ13C, δ15N, 14C dating and phytoliths) that the Podzols genesis is related to changes in vegetation and climate, occurring between the Holocene and late Pleistocene.

In this environment, the ground penetrating radar (GPR) is a tool that can contribute to the understanding of the spatial variation and arrangement (thickness, depth and transition) of the horizons of Podzols. According to the principle of GPR, the morphological differentiation between the horizons of the Podzols can be detected by the emission of different electromagnetic pulses (Ucha et al., 2010), and consequently, it can be inferred in the spatial distribution of these horizons.

The aim of the present study is to characterize the morphological, physical and chemical properties of soils (Podzol), associated with GPR data and stable C isotopes of the soil profile, across the ecotone between native grassland and Tabuleiro forest in northeastern Espírito Santo State, Brazil, in order to understand the genesis and spatial distribution of the B spodic horizon and its relation to vegetation and soil properties.

2. Study site

The study area is located in the Vale Nature Reserve (VNR), northeastern of the Espírito Santo State, Brazil. The VRN is a protected area within the natural range of the lowland Atlantic Forest, and it is one of the most important areas for biodiversity conservation (Ministério do Meio Ambiente, 2000).

The geological landscape is characterized by highland areas with Precambrian rocks, offering an uneven relief occupied by Atlantic Forest, and a system of dendritic rivers. The Neogene plateau to the east of the relief, locally called Tabuleiros Costeiros, is formed by continental deposits of the Barreiras Formation (Tertiary period), a flat terrain with a corrugated slope towards the sea. The Tabuleiros comprises marine, fluvial-marine, lagoon and eolian sediments accumulated during the Quaternary. The Tabuleiros evolution was strongly controlled by relative sea-level changes, fluvial sedimentation, long shore drift, and changes in atmospheric circulation (Martin et al., 1993).

3. Material and methods

The soil sampling was carried out in the VNR (19°11′58″ S and 40°05′22″ W. Fig. 1). The climate in the region is warm and humid, tropical type (Aw), with a rainy season in the austral summer and dry winter, mean annual precipitation of 1215 mm, mean annual temperature of 23.3 °C (Buso Junior et al. 2013). In the area of the VNR, it is possible to distinguish (with a resolution of ~5.0 m) distinct vegetation-soil relationships in circular areas of grasslands within Tabuleiro forest, with transitional shrub vegetation.

Six trenches were dug within two study areas spanning the center of the grassland to the Tabuleiro forest: transect 1 – profile P1: 19^0 09′ 11.30″ S 40^0 03′55.40″ W (grassland mussununga), P2: 19^0 09′16.20″ S 40^0 03′ 54.80″ W (shrubland mussununga), P3: 19^0 09′17.16″ S 40^0 03′55.20″ W (woodland mussununga); transect 2 – profile P4: $19^0$12′47.00″ S 39^0 57′52.00″ W (grassland mussununga), P5: $19^0$12′36.10″ S 39^0 57′40.80″W (shrubland mussununga) and P6: 19^0 12′35.34″ S 39^0 57′36.30″ W (woodland mussununga). Inside the trenches the profiles were morphologically described based on Santos et al. (2015), and samples collected from all horizons. Disturbed soil samples were air-dried, ground and sieved (fraction < 2 mm) to be used for physical and chemical analyses as described in Teixeira et al. (2017). The particle size was determined by the pipette method, using sodium hydroxide 0.1 mol L^{-1} as dispersant.

To determine and map the soil horizons and assess spatial variations in soil properties, ground-penetrating radar (GPR) was used along 15 km, with transects across a representative soil area using the TerraSIR Subsurface Interface Radar (SIR) System-3000 (Geophysical Survey Systems, Inc., Salem, New Hampshire) with 200 MHz antenna (Fig. 1). The 200-MHz frequency was chosen after in situ testing with a series of antenna frequencies (70 MHz, 400 MHz, 270 MHz and 200 MHz). The 200 MHz frequency provided the optimal balance of

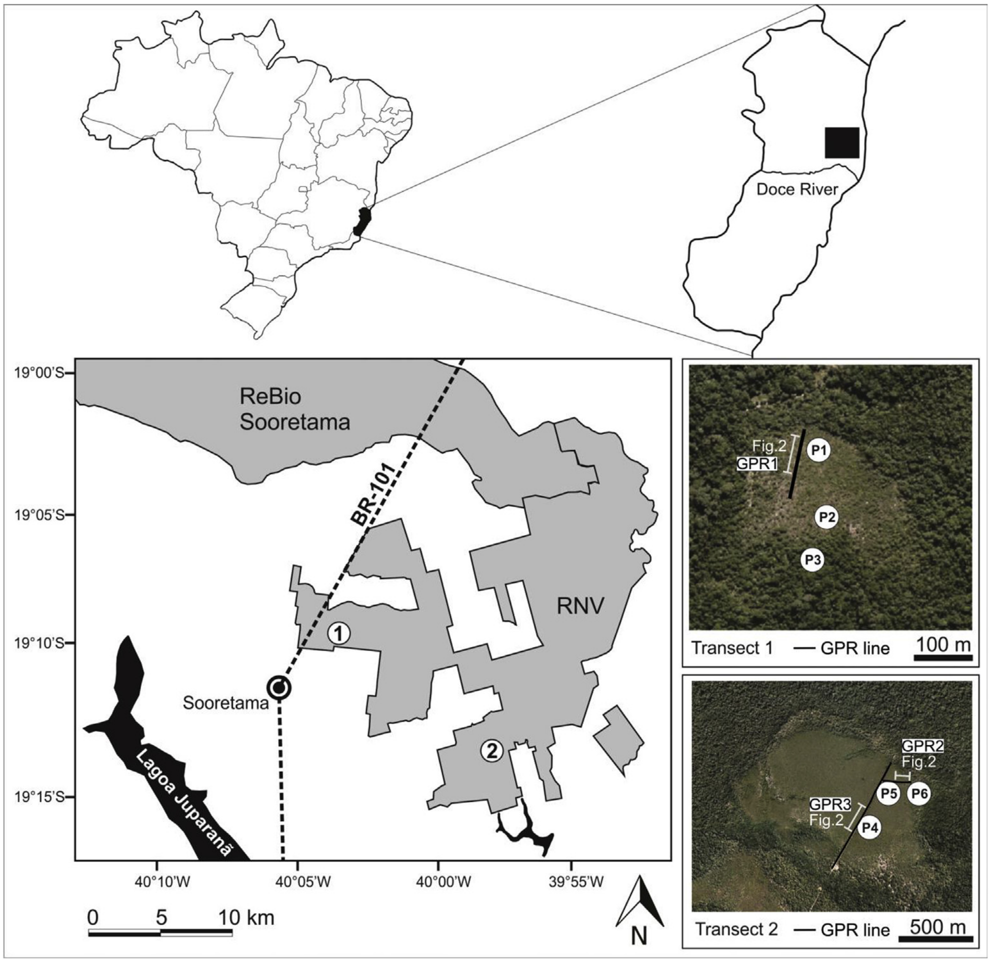

Fig. 1. Study area map showing sampling locations and Ground penetrating radar (GPR) activities in the forest grassland ecotone areas in the northeastern Espirito Santo State, Brazil. Transect 1 (profiles 1, 2 and 3) and Transect 2 (profiles 4, 5 and 6).

image quality, detection depth, and the convenience of operation in the area with both grassland and Tabuleiro forest. Traces along the GPR transects were adjusted vertically for variations in topography, using a real time kinematic global positioning system. Data processing included applying a zero time adjustment to find true ground surface reflection, same gain factor, dewow filter, a tapered bandpass filter (20–40–300–600 MHz) and an automatic gain control (AGC), using the RADAN for Windows™ software program (version 7, GSSI).

The exchangeable cations Ca^{2+}, Mg^{2+} and Al^{3+} were extracted with 1 mol L^{-1} KCl solution, the H + Al with a 0.5 mol L^{-1} calcium acetate solution with pH 7.0. For the extraction of P, Na^+ and K^+ the solution of H_2SO_4 0.0125 mol L^{-1} + HCl 0.05 mol L^{-1} was used. The levels of Ca^{2+} and Mg^{2+} were determined by titrations with 0.0125 mol L^{-1} EDTA solution; Na^+ and K by flame photometry; P by colorimetry; and Al^{3+} and H + Al, by titrations with NaOH 0.025 mol L^{-1}. The pH in water and KCl (weight 1:2.5) was determined by means of a potentiometer. The content of total organic carbon (TOC) was determined according to Yeomans and Bremner (1988). From these results, the following were calculated: the saturation by aluminum (m); the SB value (sum of exchangeable bases); T value (CTC of the ground) and V value. All the above procedures were carried out according to Teixeira et al. (2017).

The forms of Fe and Al, in their varying degrees of crystallinity, were evaluated by the use of sodium dithionite–citrate–bicarbonate (DCB) (Mehra and Jackson, 1960), and of acid ammonium oxalate (Ox), (Mckeague and Day, 1966), with determination of extracts by atomic absorption spectrometry.

The profiles P1 and P4, horizons Bhx1 (1.49–1.60 m) and Bhm1/Bhm2 (0.91–1.11 m) respectively, were selected for ^{14}C dating. These soil samples were treated according to Pessenda et al. (1996) for humin extraction. Treatments included the removal of modern roots fragments by handpicking, followed by the removal of fulvic and humic acids. The samples were combusted at the ^{14}C Laboratory and the purified CO_2 was sent to the LACUFF Laboratory, Brazil for accelerator mass spectrometry (AMS) dating (Macario et al., 2013). Ages are expressed as years before present (BP) and calibrated ages (cal. BP, 2σ), according to the SHCal13 curve (Hogg et al., 2013), using the software CALIB Rev 7.0.4 (Stuiver and Reimer, 1993) for ^{14}C age calibration.

In addition, in the profiles P1 and P4 (native grassland) soil samples were collected each 10 cm for analysis of carbon stable isotopes ($\delta^{13}C$). The profiles P1 and P4 were collected up to 1.8 m and 3.70 m, respectively. Modern root fragments were manually removed from soil samples selected for C analyses and sieved (350 μm) with distilled water to remove coarse sand grains. All samples were dried at 50 °C. Analyses were carried out at the Stable Isotope Laboratory (CENA/USP) using an elemental analyzer attached to an ANCA SL 2020 mass spectrometer. Stable isotopes ($\delta^{13}C$) were measured with respect to VPDB as standard and are expressed as *per mil* (‰) with a standard deviation of 0.2‰.

The natural oriented samples taken for micromorphological analyses were collected in horizon B spodic of the profiles P2 and P5 (0.69–0.81 m and 0.87–0.98 m, respectively), impregnated with a mixture of Polilyte polyester resin, styrene monomer, and fluorescent pigment, using Butanox as a catalyst (de Castro et al., 2003), to prepare 30-μm fine sections. The sections were observed using a polarizing

Table 1
Morphological and granulomeric attributes of soils developed in the forest grassland ecotone areas in the northeastern Espirito Santo State, Brazil.

Horizon	Depth	Munsell color		Structure[a]	Consistence			Transition[e]	Sand	Clay	Silt	Texture class
	m	moist	dry		dry[b]	moist [c]	wet[d]		g kg^{-1}			
Transect 1 - P1 – grassland												
A1	0–0.18	10 YR 3/1	10 YR 4/1	we, sm/me, gr	sf	fb	np, ss	pc	982	4	14	Sand
A2	0.18–0.36	10 YR 4/1	10 YR 5/1	sg	l	ls	np, ns	pa	970	4	26	Sand
E	0.36–1.43	10 YR 8/1	10 YR 8/1	sg	l	ls	np, ns	pa	945	2	53	Sand
Bhm1	1.43–1.49	10 YR 3/1	10 YR 5/2	massive	eh	ef	np, ns	pa	771	9	220	Loamy sand
Bhx1	1.49–1.60	10 YR 3/1	10 YR 4/2	mo, sm, ab	h	fb	np, ns	pa	683	23	294	Sandy loam
Bhx2	1.60–1.74^{+}	10 YR 3/2	10 YR 5/1	mo, sm, ab	h	fb	np, ns	–	668	29	303	Sandy loam
P2- shrubland												
A1	0–0.15	10 YR 3/1	10 YR 4/1	we, sm/me, gr	sf	fb	np, ns	pc	845	10	145	Loamy sand
A2	0.15–0.25	10 YR 4/1	10 YR 5/1	sg	l	ls	np, ns	pa	922	7	71	Sand
E	0.25–0.61	10 YR 8/1	10 YR 8/1	sg	l	ls	np, ns	pa	919	71	10	Sand
Bhm	0.61–0.74	10 YR 2/1	10 YR 3/1	massive	h	fb	np, ns	pc	723	24	253	Loamy sand
Bx1	0.74–0.98	10 YR 4/2	10 YR 5/3	massive	vh	fb	np, ns	pc	692	31	277	Sandy loam
Bx2	0.98–1.40^{+}	10 YR 5/3	10 YR 6/3	massive	vh	fb	np, ns	–	757	157	86	Loamy sand
P3 - woodland												
H	0–0.12	2,5Y 2,5/1	2,5Y 3/1	mo,sm,gr	l	ls	np, ns	pc	885	77	38	Sand
A1	0.12–0.26	2,5Y 2,5/1	2,5Y 2,5/1	sg	l	ls	np, ns	pc	912	72	16	Sand
A2	0.26–0.40	2,5Y 4/1	2,5Y 5/1	sg	l	ls	np, ns	pc	940	53	7	Sand
E1	0.40–0.57	2,5Y 5/2	2,5Y 7/1	sg	l	ls	np, ns	pa	943	40	17	Sand
E2	0.57–1.34	2,5Y 7/1	2,5Y 8/1	sg	l	ls	np, ns	pa	918	56	26	Sand
Bhm	1.34–1.41	2,5Y 5/3	2,5Y 6/3	massive	eh	f	np, ns	pc	801	75	124	Loamy sand
Bhx1	1.41–1.49	10 YR 4/2	2,5Y 5/2	massive	eh	ef	np, ns	pc	716	145	139	Loamy sand
Bhx2	1.49–1.69^{+}	2,5Y 3/1	2,5 3/1	massive	h	vf	np, ns	–	657	293	50	Sandy clay loam
Transect 2 – P4 – grassland												
A1	0–0.16	10 YR 4/1	10 YR 5/1	sg	l	ls	np, ns	pc	981	4	15	Sand
A2	0.16–0.22	10 YR 4/1	10 YR 5/1	sg	l	ls	np, ns	pc	970	4	26	Sand
E	0.22–0.91	10 YR 8/1	10 YR 8/1	sg	l	ls	np, ns	oa	945	2	53	Sand
Bhm1	0.91–0.93	10 YR 4/1	10 YR 5/2	massive	eh	vf	np, ss	pa	751	9	240	Loamy sand
Bhm2	0.93–1.11	10 YR 3/1	10 YR 3/2	massive	h	f	np, ss	pa	872	16	112	Sand
Bh	1.11–1.28^{+}	2,5Y 2,5/1	2,5Y 2,5/1	mo, sm, Bs	sf	fb	np, ns	–	610	36	354	Sandy loam
P5 – shrubland												
A1	0–0.11	10 YR 2/1	10 YR 3/1	mo, me/l, gr	sf	fb	np, ns	pc	892	10	98	Sand
A2	0.11–0.34	10 YR 3/1	10 YR 4/1	sg	l	ls	np, ns	oc	924	8	68	Sand
E	0.34–0.60	10 YR 7/1	10 YR 8/1	sg	l	ls	np, ns	pa	916	8	76	Sand
Bhm	0.60–0.70	10 YR 5/2	10 YR 5/2	massive	eh	vf	np, ns	pc	711	12	277	Loamy sand
Bh1	0.70–0.87	10 YR 2/1	10 YR 3/1	mo, sm, ab	l	ls	np, ns	pc	545	45	410	Sandy loam
Bh2	0.87–1.15	10 YR 3/2	10 YR 4/2	mo, sm, ab	h	fb	np, ss	pc	748	23	229	Loamy sand
Bh3	1.15–1.24^{+}	10 YR 3/2	10 YR 4/2	mo, sm, ab	h	fb	np, ss	–	610	36	354	Sandy loam
P6 – woodland												
A1	0–0.15	10 YR 2/2	10 YR 3/1	mo, sm, gr	sh	f	sp, ss	pc	774	183	43	Sandy loam
A2	0.15–0.34	10 YR 2/1	10 YR 3/2	mo, sm, gr	sh	f	sp, ss	pc	741	214	45	Sandy clay loam
A3	0.34–0.58	2,5Y 3/3	2,5Y 4/3	mo, sm, gr	h	f	np, ns	pc	708	262	30	Sandy clay loam
A4	0.58–0.73	2,5Y 3/2	2,5Y 5/3	mo, sm, sab	sh	fb	sp, ns	pc	732	246	22	Sandy clay loam
A5	0.73–1.00	2,5Y 3/2	2,5Y4/2	mo, sm, sab	sh	fb	sp, ns	pc	733	255	12	Sandy clay loam
Btg1	1.00–1.29	2,5Y 8/3	2,5Y 8/2	mo, sm, sab	h	f	p, s	pa	191	430	379	Clay
Btg2	1.29–1.50	2,5Y 8/3	2,5Y8/2	mo, sm, sab	h	f	p, s	pc	168	487	345	Clay
Btg3	1.50–1.82^{+}	2,5Y 8/3	2,5Y 8/2	mo, sm, sab	h	f	p, s	–	284	366	350	Clay loam

[a] Structure: degree of development: (we: weak, mo: moderate), size (sm: small, me: medium, l: large), shape (gr: granular, sg: simple grains, ab: angular blocks, sab: subangular blocks).
[b] Dry consistence: (sf: soft, l: loose, eh: extremely hard, h: hard, vh: very hard, sh: slightly hard).
[c] Moist consistence: (fb: friable, ls: loose, ef: extremely firm, f: firm, vf: very friable).
[d] Wet consistence: (np: not plastic, p: plastic; sp: slightly plastic; ss: slightly sticky, ns: not sticky).
[e] Transition: (pc: plain and clear, pa: plain and abrupt, oa: ondulation and abrupt, oc: ondulation and clear).

optical microscopic (Carl Zeiss, Lab.A1 Axio, Germany) and binocular magnifier (Carl Zeiss, 444036-9010, Germany), both under normal and polarized light. Photomicrographs were obtained using a photomicroscopic camera (Carl Zeiss, Axiocam 305 color, Germany). The micromorphological descriptions followed the criteria and terminologies proposed by Bullock et al. (1985) and Stoops (2003).

From the morphological descriptions and analytical data (chemical and physical), soils were classified according to the World Reference Base for Soil Resources (IUSS Working Group WRB, 2015), in Podzols (profiles P1, P2, P3, P4 and P5) and Acrisols (P6).

4. Results and discussion

4.1. Morphological and physical attributes

Soils described in both transects showed differences in terms of color, structure, consistence, soil thickness, transition between horizons and physical attributes (Table 1).

Except for profile P6 that has a sequence of A-Btg horizons, the other profiles showed a spodic A-E-B sequence. In these profiles, underlying the E albic horizon, the spodic B horizon appeared cemented in varying degrees, with a massive structure, characteristic of ortstein, occurring with different thicknesses and at different depths (Fig. 2). Farmer et al. (1983) indicate that this cementation occurs between the grains of quartz and organic compounds. In profiles P1, P2 and P3 the

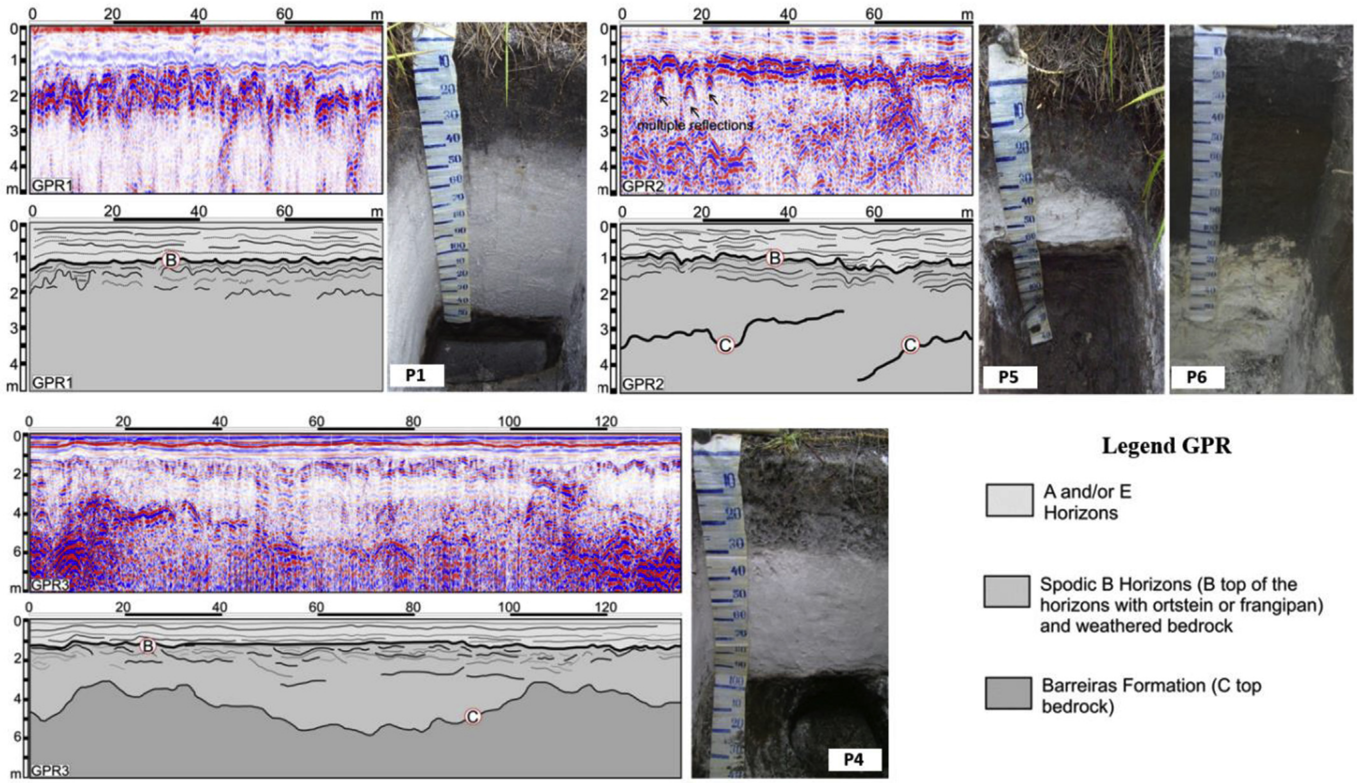

Fig. 2. Ground penetrating radar (GPR) data and interpretation of the radargram with the different soils horizons and deposits of the Barreira Formation identified in the profile.

duric horizon occurs below the spodic B horizon (Santos et al., 2015), a feature also observed by Oliveira et al. (2010) and Carvalho et al. (2013) in Podzols of the Barreiras Formation in southern Bahia and Paraíba, respectively, northeastern Brazil.

This interpretation is also supported by GPR data (Fig. 2). The GPR1 line (Fig. 2) in the transect 1 (Fig. 1) reaches up to ~2.0 m thick and shows a distinct interface between the two contrasting materials with a lateral extension of several hundreds of meters (Fig. 2). At the top of the radargram, there are continuous sand medium amplitude and sub-horizontal reflections that extend from the top of the record to 1.5 m. These reflections could be related to the A and E horizon that resulted in a lower contrast in soil electrical properties and a weaker GPR reflection, probably due to the process of the progressive illuviated silicate clays, with migration of clay-humus complexes to the underlying horizons. These conditions favor the infiltration and drainage of rainwater for the B spodic horizon (Doolittle and Collins, 1995; Burgoa et al., 1991). On the radar record, the lower part of the A-E horizon is characterized by a continuous strong reflection, showing a wavy or irregular geometry. This reflection corresponds approximately to the top of the B spodic (1.5 m depth), i.e., below of the spodic horizon, soil that contains silt or loamy particle-size classes with significant levels of moisture and organic carbon that can be related to genesis of duric horizon. The processes associated with duric horizon formation result in hydro-consolidation that causes close packing of grains and reduces porosity (Bockheim and Hartemink, 2013). The latter generates a high radar signal associated with the presence of diagnostic subsurface horizons, represented by a spodic horizon. Duric horizon has higher bulk densities and is less permeable than overlying or underlying horizons (Doolittle et al., 2005), which can be significantly attenuated by radar energy below the top of spodic horizons and no clear reflections were detectable in the lower part of the radar record (Fig. 2; GPR1).

The GPR2 line (Fig. 2) obtained between P5 and P6 trenches (Fig. 1) reaches a depth of 3 m in the soil horizons, below which are weathered deposits of the Barreiras Formation which extend to > 4 m. The high-amplitude interval lies around 1 m and shows a continuous reflecting horizon, that can be coincident with the spodic horizon in P5 and/or Btg1 in P6. The top of the profile (Fig. 2) is dominated by discontinuous low amplitude, parallel to sub-horizontal reflections which appear to be related to the A horizon which is affected by water infiltration, plant root penetration and undecomposed organic matter. These conditions favor the occurrence of water in the near-surface layer (Mendonça et al., 2015), which can reflect a discontinuity in the GPR signal at the top.

On the radargram GPR3 (Fig. 2) recorded at transect 2 (Fig. 1), the soil profile reaches 4 m, with great spatial variability in thickness (up to 6 m) and consists of three different reflection patterns. The upper part, extending to 1.5 m, contains near horizontal internal reflections with a strong amplitude signal and extends along the whole GPR profile. These stronger reflections signify a continuous A-E horizon and are interpreted as layers that contain significant accumulations of silicate clay, organic matter and Fe and Al. Below this section, down to 1 m, internal reflections change from subparallel to wavy with a concave shape and show a lateral extension of up to hundreds of meters with reflectors more segmented. While the highest amplitudes are restricted to reflections in the depth range of 0.5–1 m, reflections beneath were attenuated rapidly and are of low to very low amplitude (Fig. 2). These reflectors are attributed to cemented spodic horizons and can be associated with the presence of ortstein traced laterally on GPR lines. Cemented horizons are more compacted, with fewer pores and differences in textural properties (Doolittle and Butnor, 2009; Afshar et al., 2017) when compared to the overlapping layers and can generate high amplitude, and greater attenuation of the GPR signal. As reported by Mokma et al. (1990), the increased signal reflections from the spodic horizon can produce high amplitude reflections that are associated with the presence of ortstein. The lowermost boundaries are imaged as high-amplitude and contain subparallel to concave reflections and, lateral discontinuity, from which noises occur. This unconformity at a depth of around 4–5 m forms the lower boundary of the soil profile, which can be attributed to weathered bedrock surfaces of the Barreiras Formation in situ.

The GPR data (Fig. 2) show that the top of the spodic horizons ranges in depth from about 0.6 to 2 m and developed in response to the process of reworking of weathered deposits of the Barreiras Formation, from which the radar energy was significantly attenuated, and no clear reflections are detectable. As reported by Doolittle and Butnor (2009), because of differences in their bulk density and water retention capacity, spodic horizons are detectable with GPR.

Spodic horizons of profiles P1, P2, P3, P4 and P5 have a 10 YR matrix with dark and gray hues (low value and chroma), mainly due to the high content of organic matter, while in albic E horizons, due to the multiple pedogenetic processes of translocation, whitish colors were observed (high value). The presence of the E horizon is an indication of the pedogenetic process of leucinization which creates a lighter coloured horizon (Kämpf and Curi, 2012). In general, these profiles have a structure ranging from granular to simple grains in A and E horizons, and massive in the spodic B. Furthermore, the consistency of the surface horizons was loose, while consistency of the spodic B horizons ranged from hard to extremely hard. In general, all horizons had a wet non-plastic and non-sticky consistency. This characteristics of soil consistency is a result of the coarse grain size in the horizons. Fine sand is predominant in the profiles. The textural class ranges between sand, loamy sand, sandy loam and sandy clay loam.

The differences in the depths of spodic B horizons, observed in the two areas studied, is related to the oscillation of the water table, which is influenced by the altitude and shape of the relief (Santos et al., 2015; Coelho et al., 2010c). The GPR transect fluctuations of the reflected signal in the radargram (Fig. 2) confirmed the variation in the depth of the spodic horizon in the study areas. The largest dimensions occurred where the profile P1 is located, the level of the water table is far below the surface (> 1.0 m), and consequently, the top of the spodic B horizon is formed from 1.43 m depth, and the albic E horizon is $\sim$1.07 m thick. On the other hand, for soils in micro-depressions, the water table occurs closer to the surface (< 1.0 m) for most of the year. In these cases, as noted in the profiles P2 and P5, the albic E horizons range in thickness from 0.16 to 0.36 m and the spodic B are formed near the surface (0.60 m).

The P6 profile has a 10 YR hue in the superficial horizons, with low chroma and value, with colors ranging from dark gray brown to black. In sub-surface horizons the 2.5 Y hue is predominant, with colors ranging from light grayish brown to light yellow brown. In this profile, in superficial horizons, a granular-type structure occurs and in the sub superficial blocks, it was sub angular. A clay increment was observed with depth, with a textural gradient of 1.8 associated with the textural class clay and clay loam. The increment of clay causes the texture to be sticky and plastic when humid in the subsurface horizons of profile P6. In the GPR2 line the high reflection amplitudes up to 1 m indicate abrupt changes in wave energy which, can be attributed to an alternation in grain-size with the clay-rich B horizon.

It should be noted that in the subsurface horizons of the profiles, at a depth varying from 124 cm in profile P5 to 182 cm in P6, all material had a similar grain size, possibly as a result of the weathering in the Barreiras Formation.

4.2. Chemical attributes

The highest levels of TOC were observed in the surface horizons (horizon A and H) of all profiles, as well as in subsurface spodic B horizons of the profiles P1, P2, P3, P4 and P5, which is characteristic of the process of translocation of organic matter (Table 2). Depending on the sandy nature, the high levels of TOC influenced the sorption complex of the soils under study.

The pH values in water ranged from 3.8 on the Bhm2 horizon of profile P4, to 6.2 in the Bhx1 of profile P3, classified as extremely to moderately acidic, respectively (Santos et al., 2018). This pattern of high acidity of Podzols is related to the high values of H^+ and Al^{3+} present in the organic matter, mainly in the surface and subsurface spodic B horizons, corroborating other studies in sandbank areas (Gomes et al., 2007; Coelho et al., 2010c) and in the Barreiras Formation (Oliveira et al., 2010; Mafra et al., 2002; Silva et al., 2013; Carvalho et al., 2013).

The highest levels of P occurred in subsurface horizons, with maximum values of 117 mg kg^{-1}, in the Bx2 horizon of the P2. Oliveira et al. (2010) observed high P content in Podzols of sandbank areas in the Barreiras Formation and that P is complexed with organic matter, being translocated in the profile and piling up on the spodic B due to the sandy soil texture. In addition, the reduction of crystallinity of iron oxides (Silva et al., 2013) by organic acids also explains the accumulation of P on the spodic B horizon.

In general the values of the exchangeable cations were low, K^+ was not detectable, and Na^+, Ca^{2+} and Mg^{2+} ranged from 0 to 0.38, 0 to 2.1 and 0.1–2.9 $cmol_c$ kg^{-1}, respectively, reflecting the low values of sum and bases saturation, characteristic of the Podzols category (Dias et al., 2003; Oliveira et al., 2010; Coelho et al., 2010c; Mafra et al., 2002; Carvalho et al., 2013; Silva et al., 2013).

As with the total carbon content, the surface and B spodic horizons presented the highest levels of Al3+, H+ and H + Al, suggesting that Al complex with organic material is largely responsible for the genesis of the spodic B horizon (Van Breemen and Buurman, 1998). However, microbial degradation of organic compounds of the spodic B horizon can promote the release and increase of exchangeable Al, as noted by Oliveira et al. (2010), in agreement with the data of this study. Several studies have found high levels of Al^{3+} in the spodic B horizon in different Podzol formation environments, such as sandbank areas (Coelho et al., 2010c), the Barreiras Formation (Corrêa et al., 2008; Oliveira et al., 2010) and in the North region (Mafra et al., 2002).

The forms of crystallinity of Fe and Al varied depending on the soils, as well as on depth in the profiles (Table 3). In the profiles P1, P2, P3, P4 and P5, besides the exchangeable Al, the Al content in oxalate extracts and DCB showed an accumulation of that element in spodic B horizons. The extracts of Fe oxalate and DCB showed low levels and did not vary with soil depth, suggesting greater participation of the Al complexed to the organic acids in the process of podzolisation, during the genesis of the spodic horizon (Coelho et al., 2010c; Oliveira et al., 2010). The Al/Fe ratios are high in both extracts, highlighting the relatively greater contribution of Al compared to Fe in the formation of the spodic B horizon. In addition, the Al_{Ox}/Al_{DCB} ratio in subsurface horizons of all profiles studied was greater than the unit, indicative of the predominance of distinct forms of this element of lower crystallinity.

This pattern occurs as a result of the high levels of Al of the Barreiras Formation, as well as the hardening of the spodic horizon and the presence of duric horizon, that create an environment of water saturation, reducing and removing Fe from the system (Anderson et al., 1982; Corrêa et al., 2008; Coelho et al., 2010c; Oliveira et al., 2010; Carvalho et al., 2013; Silva et al., 2013). This process is intensified in soils of sandy texture, similar to those observed in the study area.

In the P6 profile, the Al levels were higher compared to Fe, both in DCB extracts and in oxalate, but without accumulation in specific horizons. The water table near the surface ($\sim$0.1 m) provided a sharp build-up of organic matter and formation of subsurface Btg horizon with reductomorphic characteristics, with grayish colors typical of a reducing environment and removal of Fe (Santos et al., 2018), while Al was connected to the organic matter.

4.3. *δ 13C and ^{14}C ages of soil organic matter*

The $\delta^{13}C$ of soil organic matter varied from −28.89‰ to −27.57‰ in profile P1, and -28.42‰ to −25.28‰ in the profile P4 (Fig. 3), characterizing the dominance of C_3 plants in both sites. These values are similar to those found in the modern dominant plants' species in the

Table 2
Chemical attributes of soils developed in the forest grassland ecotone areas in the northeastern Espirito Santo State, Brazil.

Horizon	Depth	TOC	pH		P	K^+	Na^+	Ca^{2+}	Mg^{2+}	H + Al	Al^{3+}	SB	T	m	V
	m	g kg^{-1}	Water	KCl	mg kg^{-1}	$cmol_c$ kg^{-1}								%	
Transect 1 - P1 – grassland															
A1	0–0.18	14.5	4.4	2.6	7	0	0.09	0.9	0.3	11.3	1.7	1.3	12.6	14	10
A2	0.18–0.36	16.7	4.4	2.7	12	0	0.01	1.0	0.2	5.6	1.3	1.2	6.8	19	18
E	0.36–1.43	3.7	5.3	4.3	1	0	0.01	0.3	0.1	0.4	0.1	0.4	0.8	12	51
Bhm1	1.43–1.49	19.0	4.0	2.8	2	0	0.01	0.2	0.2	17.8	4.5	0.4	18.2	25	2
Bhx1	1.49–1.60	26.5	4.1	3.4	33	0	0.01	0.3	0.1	33.2	4.5	0.4	33.6	13	1
Bhx2	1.60–1.74$^+$	30.5	4.2	3.6	28	0	0.01	0.3	0.1	15.0	3.1	0.4	15.4	20	3
P2- shrubland															
A1	0–0.15	14.5	4.3	2.4	13	0	0.23	2.1	1.0	26.4	2.1	3.3	29.7	7	11
A2	0.15–0.25	5.2	4.3	2.6	18	0	0.02	0.7	0.2	6.9	1.2	0.9	7.8	15	12
E	0.25–0.61	5.0	5.1	3.7	0	0	0.01	0.3	0.1	0.2	0.1	0.4	0.6	16	67
Bhm	0.61–0.74	27.5	4.0	3.0	8	0	0.06	0.4	0.1	35.9	8.6	0.6	36.5	24	2
Bx1	0.74–0.98	8.2	4.1	3.6	26	0	0.38	0.1	0.1	15.1	5.1	0.6	15.7	33	4
Bx2	0.98–1.40$^+$	9.2	4.3	3,7	117	0	0.37	0.0	0.1	14.3	3.2	0.5	14.8	22	3
P3- woodland															
H	0–0.12	92.3	4.1	2.8	21	0	0.39	0.4	2.9	22.6	4.7	3.3	25.9	41	13
A1	0.12–0.26	45.5	4.5	2.9	9	0	0	0.3	1.0	10.7	2.2	1.3	12.0	37	11
A2	0.26–0.40	21.3	4.5	3.2	9	0	0	0.4	0.2	7.6	1.5	0.6	8.2	29	7
E1	0.40–0.57	9.6	5.8	3.6	5	0	0	0.2	0.1	4.8	0.5	0.3	5.1	38	6
E2	0.57–1.34	7.0	6.0	4.6	3	0	0	0.3	0.2	4.9	0.3	0.5	5.4	63	9
Bhm	1.34–1.41	15.8	6.1	4.0	4	0	0	0.2	0.8	5.4	0.6	1.0	6.4	63	16
Bhx1	1.41–1.49	15.2	6.2	3.8	6	0	0	0.1	0.7	10.0	3.3	0.8	10.8	20	7
Bhx2	1.49–1.69$^+$	61.0	6.1	4.0	23	0	0	0.3	0.2	19.6	6.7	0.5	20.1	7	2
Transect 2 – P4 – grassland															
A1	0–0.16	8.0	4.2	2.7	5	0	0.01	0.5	0.2	5.5	0.9	0.7	6.2	14	11
A2	0.16–0.22	2.3	4.5	2.9	5	0	0.01	0.8	0.3	3.3	0.6	1.1	4.4	14	25
E	0.22–0.91	1.8	5.2	4.4	0	0	0.02	0.5	0.2	1.2	0.2	0.7	1.9	10	37
Bhm1	0.91–0.93	7.2	4.2	2.8	0	0	0.01	0.3	0.1	10.8	1.5	0.4	11.2	13	4
Bhm2	0.93–1.11	35.2	3.8	2.6	0	0	0.01	0.5	0.3	56.2	7.6	0.8	57.0	13	1
Bh	1.11–1.28$^+$	33.9	3.9	2.8	2	0	0.01	1.0	0.4	49.6	5.8	1.4	51.0	11	3
P5 – shrubland															
A1	0–0.11	6.3	3.9	2.6	11	0	0.16	0.9	0.3	16.2	2.5	1.4	17.6	14	8
A2	0.11–0.34	9.3	4.1	2.7	6	0	0.02	0.3	0.2	6.5	1.5	0.5	7.0	21	7
E	0.34–0.60	2.0	4.7	4.0	0	0	0.02	0.5	0.2	0.2	0.2	0.7	0.9	22	78
Bhm	0.60–0.70	22.5	4.2	3.2	1	0	0.02	0.2	0.1	10.6	2.9	0.3	10.9	27	3
Bh1	0.70–0.87	14.5	4.4	3.3	14	0	0.01	0.2	0.1	30.3	5.9	0.3	30.6	19	1
Bh2	0.87–1.15	18.2	4.4	3.8	29	0	0.01	0.1	0.1	12.4	2.5	0.2	12.6	20	2
Bh3	1.15–1.24$^+$	25.5	4.3	3.7	13	0	0.01	0.3	0.1	11.9	3.1	0.4	12.3	25	3
P6 – woodland															
A1	0–0.15	58.5	4.5	3.6	13	0	0.14	0.3	0.1	12.1	2.5	0.4	12.5	14	3
A2	0.15–0.34	38.1	4.7	3.8	11	0	0.32	0.4	0.3	15.0	2.4	0.7	15.7	23	4
A3	0.34–0.58	58.8	4.9	4.1	8	0	0.12	0.3	0.1	24.0	3.0	0.4	24.8	12	2
A4	0.58–0.73	48.7	5.0	4.2	6	0	0.12	0.3	0.1	18.2	1.9	0.4	18.6	17	2
A5	0.73–1.00	37.0	5.0	4.3	6	0	0.14	0.3	0.1	14.5	1.8	0.4	14.9	18	3
Btg1	1.00–1.29	16.4	5.0	4,1	4	0	0.08	0.3	0.2	8.0	1.7	0.5	8.5	23	6
Btg2	1.29–1.50	17.2	5.0	4.2	4	0	0.00	0.3	0.2	6.6	2.0	0.5	7.1	20	7
Btg3	1.50–1.82$^+$	21.1	4.9	4.1	5	0	0.06	0.3	0.1	6.0	1.5	0.4	6.4	21	6

TOC: total organic carbono (method of Yeomans e Bremner); pH em água e KCl (1:2,5); P, K e Na: extracted by Mehlich-1; Ca, Mg e Al: extracted by KCl 1 mol L^{-1}; H + Al: extracted by calcium acetate 0,5 mol L^{-1} pH 7,0; SB: bases of sum; m: saturation by aluminum; V: saturation by bases.

areas of profiles P1 (*Renvoizea trinii*) and P4 (*R. trinni* and *Lagenocarpus rigidus*), which are C_3 plants and present $\delta^{13}C$ of −28.9‰ and −28.4‰, respectively (Buso Junior et al., 2013). Enriched values of $\delta^{13}C$ observed in the B spodic horizons (P1 = −27.57‰; P4 = −25.28‰) may be related to the isotopic fractionation resulted from organic matter decomposition (Macko and Estep, 1984) and do not reflect changes in relative abundance of C_3 and C_4 plants.

The ^{14}C ages obtained from the humin in the B spodic horizons varied from 38,890 to 14,251 cal BP in profiles P1 and P4, respectively. Then, ^{14}C ages and $\delta^{13}C$ values indicate that C_3 plants dominate the vegetation of the studied sites at least since the late Pleistocene.

Considering the organic matter in the B spodic horizon as a mixture of humin fractions with different ages, the ^{14}C ages obtained may reflect the minimum age, an aspect also recorded by Perrin et al. (1964). They considered that in biologically inert B spodic horizons of tropical oligotrophic Podzols, with low organic matter cycling, the ^{14}C ages would reflect the minimum age of formation of these horizons. Buurman and Jongmans (2005) argued that oligotrophic Podzols in the tropical region, with reduced biologic activity, present longer residence time of the organic matter in the B spodic horizon. Consequently, the difference in the ages between P1 and P4 profiles would indicate differences in the time of formation of the Podzols and/or in the vegetation covering in both sites. A similar situation was observed by Schwartz (1988) in Podzols in Congo, with ages varying from ~40,000 to 10,000 years BP.

In relation to environmental conditions that may lead to Podzol formation, Schwartz (1988) related the ages of formation of spodic horizons with the time intervals of more humid climates in Congo. Dubroeucq and Volkoff (1998) suggested that the process of Podzols formation in the Rio Negro basin would involve, in its initial stages, the acidic hydrolysis of clay minerals by the soil solution. This initial process may be favored by higher environmental humidity, consequently, the palaeoenvironmental conditions that led to the initial formation of the B spodic horizons were related to the time intervals of predominant humid climates during late Pleistocene (at ~40,000 cal BP and ~14,000 cal BP).

Table 3
Fe e Al extracted by oxalate (Ox) and dithionite-citrate-bicarbonate (DCB) and the ratio of these metals of soils developed in the forest grassland ecotone areas in the northeastern Espirito Santo State, Brazil.

Horizon	Depth	Oxalate			DCB			Al_{ox}/Al_{DCB}	Fe_{ox}/Fe_{DCB}
		Al	Fe	Al/Fe	Al	Fe	Al/Fe		
	m	g kg^{-1}			g kg^{-1}				
Transect 1 - P1 – grassland									
A1	0–0.18	0.02	0.02	0.68	0.00	0.48	0.00	0.00	0.05
A2	0.18–0.36	0.00	0.01	0.00	0.00	0.45	0.00	0.00	0.02
E	0.36–1.43	0.00	0.00	0.00	0.00	0.58	0.00	0.00	0.01
Bhm1	1.43–1.49	0.90	0.01	87.94	0.62	0.52	1.21	1.44	0.02
Bhx1	1.49–1.60	3.38	0.01	413.47	4.06	0.52	7.77	0.83	0.02
Bhx2	1.60–1.74^{+}	2.59	0.04	58.59	1.71	0.47	3.68	1.51	0.09
P2- shrubland									
A1	0–0.15	0.16	0.04	4.04	0.04	0.95	0.04	4.07	0.04
A2	0.15–0.25	0.03	0.02	1.48	0.00	0.87	0.00	0.00	0.02
E	0.25–0.61	0.00	0.01	0.00	0.00	0.83	0.00	0.00	0.01
Bhm	0.61–0.74	3.78	0.05	69.51	4.29	0.90	4.78	0.88	0.06
Bx1	0.74–0.98	2.89	0.02	117.26	1.91	0.73	2.61	1.51	0.03
Bx2	0.98–1.40^{+}	5.26	0.03	167.68	3.49	0.88	3.96	1.51	0.04
P3- woodland									
H	0–0.12	0.02	0.04	0.43	0.27	0.47	0.58	0.07	0.09
A1	0.12–0.26	0.02	0.01	1.44	0.23	0.53	0.45	0.09	0.03
A2	0.26–0.40	0.01	0.01	0.95	0.18	0.47	0.38	0.05	0.02
E1	0.40–0.57	0.00	0.00	0.41	0.13	0.39	0.35	0.01	0.01
E2	0.57–1.34	0.00	0.00	0.25	0.29	0.49	0.59	0.00	0.01
Bhm	1.34–1.41	0.05	0.04	1.09	0.56	0.56	1.00	0.08	0.08
Bhx1	1.41–1.49	0.99	0.05	17.99	1.14	0.45	2.55	0.87	0.12
Bhx2	1.49–1.69^{+}	6.24	0.19	33.33	3.85	0.40	9.55	1.62	0.46
Transect 2 – P4 – grassland									
A1	0–0.16	0.00	0.02	0.00	0.00	0.42	0.00	0.00	0.05
A2	0.16–0.22	0.00	0.01	0.00	0.00	0.56	0.00	0.00	0.02
E	0.22–0.91	0.00	0.00	0.00	0.00	0.55	0.00	0.00	0.01
Bhm1	0.91–0.93	0.49	0.03	15.88	0.28	0.46	0.61	1.76	0.07
Bhm2	0.93–1.11	3.48	0.01	241.19	3.48	0.51	6.88	1.00	0.03
Bh	1.11–1.28^{+}	3.28	0.01	247.33	3.65	0.61	6.03	0.90	0.02
P5 – shrubland									
A1	0–0.11	0.08	0.10	0.82	0.00	0.68	0.00	0.00	0.15
A2	0.11–0.34	0.05	0.04	1.17	0.00	0.43	0.00	0.00	0.10
E	0.34–0.60	0.00	0.01	0.00	0.00	0.41	0.00	0.00	0.01
Bhm	0.60–0.70	0.83	0.03	23.81	0.91	0.61	1.50	0.91	0.06
Bh1	0.70–0.87	4.85	0.04	129.02	5.70	0.50	11.43	0.85	0.08
Bh2	0.87–1.15	2.22	0.02	136.38	2.37	0.74	3.19	0.93	0.02
Bh3	1.15–1.24^{+}	1.77	0.02	76.26	1.51	0.67	2.26	1.17	0.03
P6 – woodland									
A1	0–0.15	1.15	0.22	5.15	1.50	0.66	2.27	0.77	0.34
A2	0.15–0.34	2.40	0.15	16.49	1.90	0.48	3.97	1.26	0.30
A3	0.34–0.58	18.23	0.62	29.44	15.48	0.70	21.97	1.18	0.88
A4	0.58–0.73	11.25	0.34	33.34	11.02	0.67	16.37	1.02	0.50
A5	0.73–1.00	8.57	0.14	61.95	7.12	0.45	15.68	1.20	0.30
Btg1	1.00–1.29	5.13	0.57	9.05	3.44	0.84	4.09	1.49	0.68
Btg2	1.29–1.50	3.56	0.42	8.39	2.47	0.78	3.16	1.44	0.54
Btg3	1.50–1.82^{+}	3.34	0.31	10.88	2.39	0.65	3.67	1.40	0.47

Some palaeoenvironmental studies have suggested similar humid intervals for the palaeoclimate in southeastern Brazil. Based on pollen analysis, Ledru et al. (1996), at Serra do Salitre, Minas Gerais State, ~1200 km west of VNR, suggested high moisture levels during the interval 40,000-27,000 BP (44,151–30,709 cal BP), with a maximum humidity at ~35,000 BP (40,095-38,843 cal BP). In the same study, the authors inferred the gradual increase in the humidity after the late Glacial, during the interval 16,000–11,000 BP (19,741–12,545 cal BP). Pessenda et al. (2009), at the Curucutu Nature Reserve, São Paulo State, ~1000 km south of VNR, used pollen analysis in a peatland and C isotopes in the soil organic matter, to infer the presence of a humid climate for the interval 28,000–15,000 BP (~31,500 - 18,000 cal BP), characterizing the expansion of Araucaria forest in the region, today located ~500 km to the south, at Paraná State. Veríssimo et al. (2012) studied a pollen record in the Serra do Caparaó, ~230 km from VNR, and inferred humid climate for the transition Pleistocene – Holocene (~11,500 cal BP). Based on $\delta^{18}O$ of stalagmites from south and southeastern Brazil, Cruz Jr et al. (2005, 2006) suggested intervals of higher rainfall amounts around 45,000–40,000 (~48,000–43,000 cal BP) and 20,000–14,000 BP (~24,000–17,000 cal BP) in the Bt2 record, and around 47,000–37,000 (~50,000–40,000 cal BP) and 20,000–15,500 (~24,000–18,500 cal BP) in the St8 record, caused by changes in the location and/or convective activity of the South American summer monsoon.

4.4. Micromorphology and genesis of soils

The spodic horizons had similar micromorphological features (Table 4). Many areas observed in the thin sections had organic matter coatings completely filling the porous space, with a porphyric distribution pattern (Fig. 4c and e), a phenomenon already observed by Coelho et al. (2012) in spodic horizons formed in sandy materials from the coast of São Paulo state, Brazil. However, basic types of relative distribution such as chitonic, gefuric and enaulic can be observed in the

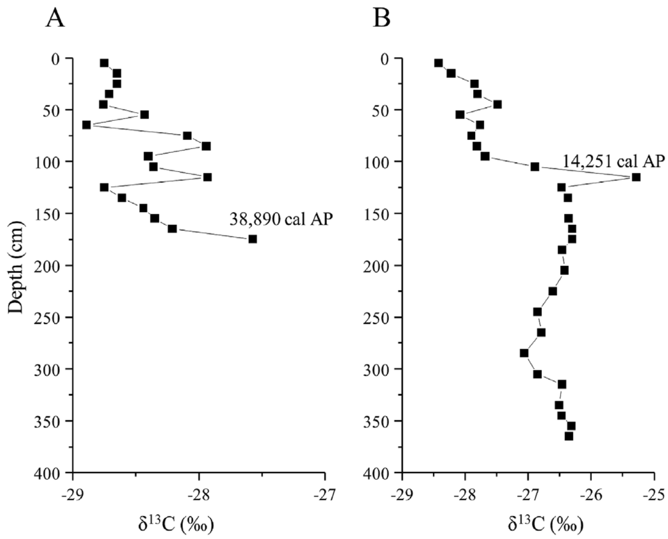

Fig. 3. Variation of δ 13C (‰) and ^{14}C ages in profiles P1 (A) and P4 (B) of Podzols in the northeastern Espirito Santo State, Brazil.

thin sections of the spodic B horizons (Fig. 4a). The organic matter in the spodic horizons, characterized by the advanced stage of transformation and absence of cellular structures or original forms of vegetable remnants, can be identified as monomorphic (De Coninck et al., 1974; Coelho et al., 2012).

In the studied horizons, there is a predominance of porosity cavity poly-concave, and the pores between the coarse grains of sub-rounded polycrystalline quartz (Fig. 4d) are filled with a fine organic matter of black tones in the central part and reddish at the extremities (Fig. 4e). This change in coloration evolves with the formation of channels and micro fissures (Fig. 4f), with subsequent separation of these constituents into smaller units, giving rise to complex microstructure with film bridges between grains and massive (Fig. 4b).

In the study environment, the combination of factors such as excess moisture, temperature and high acidity, sediment of the Barreiras Formation and flat relief, contribute to the occurrence of the pedogenetic processes of ferrolysis (Dubroeucq and Volkoff, 1998; Moreau et al., 2006) and podzolisation (Lundström et al., 2000; Corrêa et al., 2008; Oliveira et al., 2010; Silva et al., 2013). In the area covered by forest vegetation (profile P6), one may infer that these processes are largely responsible for the transformation of sedimentary material from the Barreiras Formation, with destruction of clays by the ferrolysis process. This results in more sandy surface horizons followed by other clayey subsurface horizons and the formation of Acrisols.

In a lateral transformation sequence in Acrisols located in the higher parts of the study site, the ferrolysis at the top of the Bt horizon favored by the excess of moisture in this area of the profile, leads to the formation and thickening of the E horizon, at the expense of the Bt horizon (Mafra et al., 2002; Silva et al., 2013).

At a later stage, or simultaneously to the ferrolysis, the process of podzolisation takes place, in which organic compounds such as dissolved humic and fulvic acids, complex and remove metals, mainly Fe and Al, from the superficial horizons (A, H), translocating and depositing them in the subsurface horizons and forming the spodic B (Mafra et al., 2002; Oliveira et al., 2010; Silva et al., 2013). These processes can be noted in the profiles P1, P2, P3, P4 and P5, located in the areas with grass vegetation, where there is a larger drainage impediment layer. Oliveira et al. (2010) have pointed out that the Podzols of the Barreiras Formation have a cemented spodic B horizon (Ortstein), which appears to have been formed due to the lateral transport of silica and aluminum, related to the destruction of clays from the duric horizons of Acrisols and Ferralsols, located in the higher portions of the landscape, as observed in the study area. In tropical conditions, which characterize our study, in sandy and poorly drained soil, the spodic B horizon contains plenty of organic complexes and Al, but little Fe oxides, which were reduced and removed by leaching.

The monomorphic predominance of the organic constituents evidences the mobilization, illuviation and precipitation of the organic matter in the genesis of the spodic horizon (De Coninck et al., 1974; De Coninck, 1980; Buurman et al., 2005; Coelho et al., 2012). The ^{14}C ages indicate that the accumulation of organic material of C_3 plants from the vegetation cover in B spodic horizons occurred since at least ~14,250 to 38,890 cal BP, in the profiles P4 and P1, respectively. These B horizons cause high-amplitude reflections in the GPR data, indicative of abrupt changes in wave energy, that are attributed to the formation of a cemented or indurated soil, with orstein and duric horizon.

It is assumed that the genesis of the spodic horizons occurred in the past under accentuated hydromorphism (De Coninck, 1980; Mckeague and Wang, 1980; Coelho et al., 2012). In Amazonian, the most waterlogged zones of the podzolized areas are the main source of dissolved organic matter, with an organic carbon accumulation rate in the Bh horizon of 0.54–3.17 g cm-2 year-1, which requires a long time for organic matter stabilization, whose 14C dating in the B spodic horizons ranged from 48,000 to 450,000 years BP (Doupoux et al., 2017). On the other hand, changes in the precipitation pattern, with greater frequency of dry periods, resulting in less frequent waterlogging, decrease carbon flux to the Bh horizon (Sierra et al., 2013), promoting instability and degradation of organic matter mainly at the top of the B spodic horizon (Coelho et al., 2012). This hypothesis is supported by the fact that the differentiated coloration of organic matter in the voids is associated with different degrees of decomposition, indicating differences in the chemical constituents of this organic material (Buurman et al., 2005;

Table 4
Main micromorphological characteristics of the subsurface horizons of soils developed in the forest grassland ecotone areas in the northeastern Espirito Santo State, Brazil.

	Transect 1. Profile P2- grasses. Bhm - Bx1. 0.61–0.98 m.	Transect 2. Profile P5- grasses. Bh2. 0.87–1.15 m.
Matrix	Coarse material: 65% Fine material: 20% Porosity: 15%	Coarse material: 50% Fine material: 35% Porosity: 15%
Relative distribution	Complex: chitonic-gefuric-porphyric.	Complex: porphyric-enaulic.
Coarse material	Composed of polycrystalline quartz grains, sub-rounded, subangular, smooth/wavy, sub sphere and poorly selected. Frequency: dominant (60–70%).	Composed of polycrystalline quartz grains, sub-rounded, subangular, smooth/wavy, sub sphere and poorly selected. Frequency: dominant (60–70%).
Fine material	Predominantly organic matter and clay	Clay, iron oxide and mainly organic matter.
Pores	Porosity cavity, poly-concave, with irregular cavities, channels, fissures and microfissures. Presence of some stacking pores	Porosity cavity, poly-concave, stacking. Some channels and microfissures in the fine material.
Microstructure	Complex: Film (organic matter and clay) with bridges and massive.	Complex: polyhedral microgranular aggregates with presence of coalesced zones forming a dense mass
Birefringent fabric	Undifferentiated	Undifferentiated
Pedological features	Grains covered by cutans of organic material.	Grains covered by cutans of organic material.

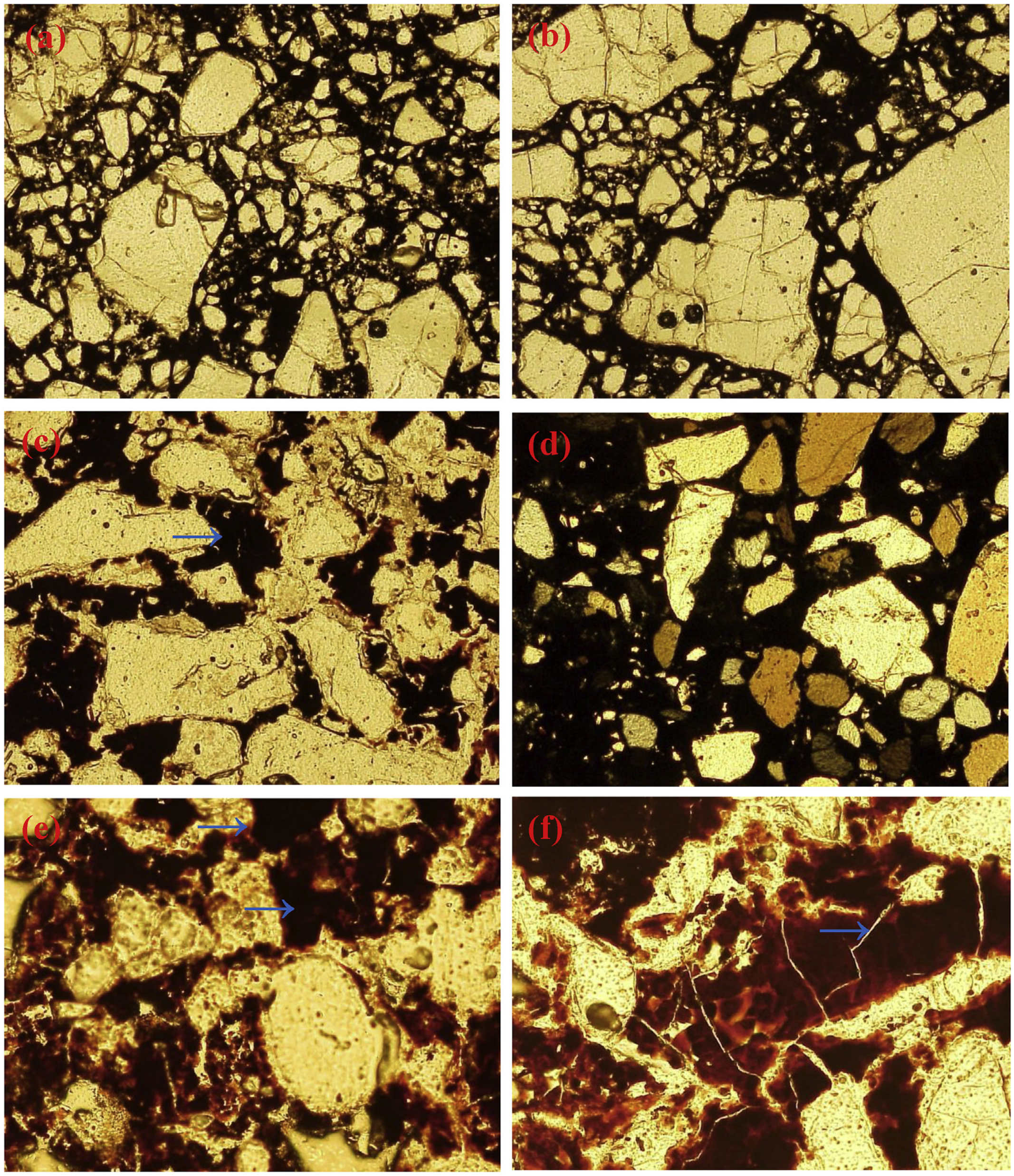

Fig. 4. Photomicrographs in which can be observed: Horizon Bhm profile P2: (a) relative distribution chitonic-gefuric-porphyric; (b) complex pellicular microstructure with bridges and massive. Horizon Bh2 profile P5: (c) monomorphic organic matter completely filling the porosity (relative distribution g/$f_{2\mu m}$ porphyric); (d) coarse material, with quartz grains and porosity cavity poly-concave; (e) fine organic material filling the voids space, with dark coloration in the central part and reddish at the extremities; (f) presence of microfissures and dissolution of fine organic material.

Bardy et al., 2008). In an evolutionary stage of decomposition of the organic matter, the microfissures are formed, which evolve originating the voids space inter-grains of the cavity poly-concave type, initiating the process of destruction of the top B spodic horizon.

5. Conclusions

The ground penetrating radar images showed that development of soil horizons occurs directly over the weathered bedrock of the Barreiras Formation. The horizons in the top of radargrams were differentiated by changes in the internal geometry of the reflectors and are consistent with the findings of the soil pedons. The data also showed that spodic horizons in transects 1 and 2 have variable thicknesses, which possibly correlate with podzolisation processes, which reflect the lateral changes of the depth and degree of weathering of the Barreiras Formation. The combination of a near-surface water table, humidity and excessive acidity and sandy nature of the sediment of the Barreiras Formation, have favoured the processes of ferrolysis and podzolisation. The destruction of clays and eluviation of organic matter complexed with aluminum provided the genesis of Acrisols and Podzols, respectively. The filling of the voids space by organic constituents evidences the process of illuviation of the organic matter, responsible for the genesis of the B spodic horizons. The accumulation of organic compounds in the B spodic horizons of the P1 and P4 profiles originated from C_3 plants, suggests the dominance of humid climate in the region since at least 38,890 cal BP.

Acknowledgments

To FUNDECT; to the CNPq/CAPES for the financial support through projects: “Casadinho” process 620029/20080 and “Casadinho/Procad” process 552377/2011-2; to CNPq (470210/2012-5, 302711/2013-9) and FAPESP (2007/03615-5, 2010/18091-4 and 2011/00995-7) for the financial support for the field trips and analyses.

Appendix A. Supplementary data

Supplementary data to this article can be found online at https://doi.org/10.1016/j.jsames.2019.102435.

References

Afshar, A.F., Ayoubi, S., Castrignanò, A., Quarto, R., Ardekani, M.R.M., 2017. Using ground-penetrating radar to explore the cemented soil horizon in an arid region in Iran. Near Surf. Geophys. 15, 103–110.
Anderson, H.A., Berrow, M.L., Farmer, V.C., Hepburn, A., Russel, J.D., Walker, A.D., 1982. A reassessment of podzol formation processes. J. Soil Sci. 33 (1), 125–136.
Bardy, M., Fritsch, E., Derenne, S., Allard, T., do Nascimento, N.R., Bueno, G.T., 2008. Micromorphology and spectroscopic characteristics of organic matter in waterlogged podzols of the upper Amazon basin. Catena 145, 222–230.
Bockheim, J.G., Hartemink, A.E., 2013. Soils with fragipans in the USA. Catena 104, 233–242.
Boski, T., Angulo, R.J., Souza, M.C., Barboza, E.G., Knicker, H., González-Pérez, J.A., González-Vila, F.J., 2015. Progradation rates of coastal barrier sands estimated from the 14C age of soil organic matter. J. Quat. Sci. 30, 9–18.
Bullock, P., Fedoroff, N., Jongerius, A., Stoops, G., Tursina, T., 1985. Handbook for Soil Thin Section Description. Waine Research Publications, Wolverhampton, pp. 152.
Burgoa, B., Mansell, R.S., Sawka, G.J., Nkedi-Kizza, P., Capece, J., Campbell, K., 1991. Spatial variability of depth to Bh horizon in Florida Haplaquods using ground-penetrating radar. Soil Crop Sci. Soc. Florida Proc. 50, 125–130.
Buso Junior, A.A., Pessenda, L.C.R., De Oliveira, P.E., Giannini, P.C.F., Cohen, M.C.L., Volkmer-Ribeiro, C., Oliveira, S.M.B., Rossetti, D.F., Lorente, F.L., Borotti Filho, M.A., Schiavo, J.A., Bendassolli, J.A., França, M.C., Guimarães, J.T.F., Siqueira, G.S., 2013. Late Pleistocene and Holocene vegetation, climate dynamics, and Amazonian taxa in the Atlantic forest, Linhares, SE Brazil. Radiocarbon 55 (2–3), 1747–1762.
Buso Junior, A.A., Pessenda, L.C.R., Mayle, F.E., Lorente, F.L., Volkmer-Ribeiro, C., Schiavo, J.A., Pereira, M.G., Bendassolli, J.A., Macario, K.C.D., Siqueira, G.S., 2019. Paleovegetation and paleoclimate dynamics during the last 7000 years in the Atlantic Forest of Southeastern Brazil based on palynology of a waterlogged sandy soil. Rev. Palaeobot. Palynol. 264, 1–10.
Buurman, P., Jongmans, A.G., 2005. Podzolisation and soil organic matter dynamics. Geoderma 125, 71–83.
Buurman, P., van Bergen, P.F., Jongmans, A.G., Meijer, E.L., Duran, B., Van Lagen, B., 2005. Spatial and temporal variation in podzol organic matter studied by pyrolysis-gas chromatography/mass spectrometry and micromorphology. Eur. J. Soil Sci. 56, 253–270.
Buurman, P., 1984. Podzols. Van Nostrand Reinhold Soil Science Series, New York (450 pp).
Buurman, P., Vidal-Torrado, P., Martins, V.M., 2013. The podzol hydrosequence of Itaguaré (Sao Paolo, Brazil). 1. Geomorphology and interpretation of profile morphology. Soil Sci. Soc. Am. J. 77, 1294–1306.
Calegari, M.R., Madella, M., Brustolin, L.T., Pessenda, L.C.R., Buso Júnior, A.A., Francisquini, M.I., Bendassolli, J.A., Vidal-Torrado, P., 2017. Potential of soil phytoliths, organic matter and carbon isotopes for small-scale differentiation of tropical rainforest vegetation: a pilot study from the campos nativos of the Atlantic Forest in Espírito Santo State (Brazil). Quat. Int. 437, 156–164.
Carvalho, V.S., Ribeiro, M.R., Souza Júnior, V.S., Brilhante, S.A., 2013. Caracterização de Espodossolos dos Estados da Paraíba e do Pernambuco, Nordeste do Brasil. Rev. Bras. Ciência do Solo 37, 1454–1463.
Coelho, M.R., Martins, V.M., Vidal-Torrado, P., Souza, C.R.G., Perez, X.L.O., Vásquez, F.M., 2010 b b. Relação solo-relevo-substrato geológico nas restingas da planície costeira do Estado de São Paulo. Rev. Bras. Ciência do Solo 34 (2), 833–846.
Coelho, M.R., Vidal-Torrado, P., Perez, X.L.O., Martins, V.M., Vázquez, F.M., 2010c. Fracionamento do Al por técnicas de dissoluções seletivas em Espodossolos da planície costeira do estado de São Paulo. Rev. Bras. Ciência do Solo 34 (2), 1081–1092.
Coelho, M.R., Martins, V.M., Pérez, X.L.O., Vázquez, F.M., Gomes, F.H., Cooper, M., Vidal-Torrado, P., 2012. Micromorfologia de horizontes Espódicos nas restingas do Estado de São Paulo. Rev. Bras. Ciência do Solo 36, 1380–1394.
Corrêa, M.M., Ker, J.C., Barrón, V., Torrent, J., Fontes, M.P.F., Curi, N., 2008. Propriedades cristalográficas de caulinitas de solos do ambiente tabuleiros costeiros, Amazônia e Recôncavo Baiano. Rev. Bras. Ciência do Solo 32 (3), 1857–1872.
Cruz Jr., F.W., Burns, S.J., Karmann, I., Sharp, W.D., Vuille, M., Cardoso, A.O., Ferrari, J.A., Dias, P.L.S., Viana Jr., O., 2005. Insolation-driven changes in atmospheric circulation over the past 116,000 years in subtropical Brazil. Nature 434, 63–66.
Cruz Jr., F.W., Burns, S.J., Karmann, I., Sharp, W.D., Vuille, M., 2006. Reconstruction of regional atmospheric circulation features during the late Pleistocene in subtropical Brazil from oxygen isotope composition of speleothems. Earth Planet. Sci. Lett. 248, 495–507.
Dantas, J.S., Marques Júnior, J., Martins Filho, M.V., Resende, J.M.A., Camargo, L.A., Barbosa, R.S., 2014. Gênese de solos coesos do leste maranhense: relação solo-paisagem. Rev. Bras. Ciência do Solo 38 (3), 1039–1050.
de Castro, S.S., Cooper, M., Santos, M.C., Vidal-Torrado, P., de Lima, J.M., 2003. Micromorfologia do solo: bases e aplicações. In: In: Curi, N., Marques, J.J., Guilherme, L.R.G., Lopes, A.S., Alvarez Venegas, V.H. (Eds.), Tópicos Em Ciência Do Solo, vol. 3. Sociedade Brasileira de Ciência do Solo, Viçosa, MG, pp. 107–164.
De Coninck, F., 1980. Major mechanisms in formation of spodic horizons. Geoderma 24, 101–126.
De Coninck, F., Righi, D., Maucorps, J., Robin, A.M., 1974. Origin and micromorphology nomenclature of organic matter in sandy spodosols. In: Rutheford, G.K. (Ed.), Soil Microscopy. Ontario. Limestone Press, pp. 263–273.
Dias, H.C.T., Schaefer, C.E.G.R., Fernandes Filho, E.I., Oliveira, A.P., Michel, R.F.M., Lemos, J.B., 2003. Caracterização de solos Altimontanos em dois transectos no Parque Estadual do Ibitipoca (MG). Rev. Bras. Ciência do Solo 27 (2), 469–481.
Doolittle, J.A., Collins, M.E., 1995. Use of soil information to determine application of ground-penetrating radar. J. Appl. Geophys. 33, 101–108.
Doolittle, J.A., Butnor, J.R., 2009. Soils, peatlands and biomonitoring. In: Jol, H.M. (Ed.), Ground Penetrating Radar: Theory and Applications. Elsevier, Amsterdam, Netherlands, pp. 179.
Doolittle, J., Daigle, J., Kelly, J., Tuttle, W., 2005. Using GPR to characterize plinthite and ironstone layers in Ultisols. Soil Surv. Horiz. 46 (4), 179–184.
Doupoux, C., Merdy, P., Montes, R.C., Nunan, N., Melfi, A.J., Pereira, O.J.R., Lucas, Y., 2017. Modelling the genesis of equatorial podzols: age and implications for carbon fluxes. Biogeosciences 14 (1), 2429–2440.
Dubroeucq, D., Volkoff, B., 1998. From Oxisols to Spodosols and Histosols: evolution of the soil mantles in the rio Negro basin (Amazonia). Catena 32 (1), 245–280.
Farmer, V.C., Russel, J.D., Smith, B.F.L., 1983. Extraction of inorganic forms of translocated Al, Fe and Si from a Podzol Bs horizon. Eur. J. Soil Sci. 34 (3), 571–576.
Gomes, F.H., Vidal-Torrado, P., Macías-Vazquez, F., Gherardi, B., Otero, X.L., 2007. Solos sob vegetação de restinga na Ilha do Cardoso-SP: I- Caracterização e classificação. Rev. Bras. Ciência do Solo 31 (4), 1563–1580.
Hogg, A.G., Hua, Q., Blackwell, P.G., Niu, M., Buck, C.E., Guilderson, T.P., Heaton, T.J., Palmer, J.G., Reimer, P.J., Reimer, R.W., Turney, C.S.M., Zimmerman, S.R.H., 2013. SHCal13 Southern Hemisphere calibration, 0-50,000 years cal BP. Radiocarbon 55 (4), 1889–1903.
Horbe, A.M.C., Horbe, M.A., Suguio, K., 2004. Tropical Spodosolsin northeastern Amazonas state, Brazil. Geoderma 119, 55–68.
IUSS Working Group WRB, 2015. World Reference Base for Soil Resources 2014, Update 2015. International Soil Classification System for Naming Soils and Creating Legends for Soil Maps. World Soil Resources Reports No. 106. FAO, Rome 1-192 pp.
Kaczorek, D., Sommer, M., Andruschkewitsch, L., Oktaba, L., Czerwinski, Z., Stahr, K., 2004. A comparative micromorphological and chemical study of "Raseneisenstein"(bog iron ore) and "Orstein". Geoderma 121, 83–94.
Kämpf, N., Curi, N., 2012. Formação e evolução do solo (Pedogênese). In: Ker, J.C., Curi, N., Schaefer, C.E.G.R., Vidal Torrado, P. (Eds.), Pedologia: Fundamentos, 1[a] ed. SBCS, Viçosa, pp. 207–302.
Ledru, M.-P., Braga, P.I.S., Soubiès, F., Fournier, M., Martin, L., Suguio, K., Turcq, B., 1996. The last 50,000 years in the Neotropics (Southern Brazil): evolution of vegetation and climate. Palaeogeogr. Palaeoclimatol. Palaeoecol. 123, 239–257.
Lima Neto, J.A., Ribeiro, M.R., Corrêa, M.M., Souza Júnior, V.S., Lima, J.F.W.F., Ferreira, R.F.A.L., 2009. Caracterização e gênese do caráter coeso em Latossolos Amarelos e Argissolos dos Tabuleiros Costeiros do Estado de Alagoas. Rev. Bras. Ciência do Solo 33 (4), 1001–1011.
Lopes-Mazzetto, J.M., Schellekens, J., Pablo Vidal-Torrado, P., Buurman, P., 2018. Impact of drainage and soil hydrology on sources and degradation of organic matter in tropical coastal podzols. Geoderma 330, 79–90.
Lundstrom, U.S., van Breemen, N., Bain, D.C., van Hees, P.A.W., Giesler, R., Gustafsson, J.P., Ilvesniemi, H., Karltun, E., Melkerud, P.A., Olsson, M., Riise, G., Wahlberg, O., Bergelin, A., Bishop, K., Finlay, R., Jongmans, A.G., Magnusson, T., Mannerkoski, H., Nordgren, A., Nyberg, L., Starr, M., Tau Srand, L., 2000. Advances in understanding the podzolization process resulting from a multidisciplinary study of three coniferous forest soils in the Nordic Countries. Geoderma 94, 335–353.
Macario, K.D., Gomes, P.R.S., Anjos, R.M., Carvalho, C., Linares, R., Alves, E.Q., Oliveira, F.M., Castro, M.D., Chanca, I.S., Silveira, M.F.M., Pessenda, L.C.R., Moraes, L.M.B., Campos, T.B., Cherkinsky, A., 2013. The Brazilian AMS radiocarbon laboratory (LAC-UFF) and the intercomparison of results with CENA and UGAMS. Radiocarbon 55 (2–3), 325–330.
Mafra, A.L., Miklós, A.A.W., Volkoff, B., Melfi, A.J., 2002. Pedogênese numa seqüência Latossolo-Espodossolo na região do alto rio negro, Amazonas. Rev. Bras. Ciência do Solo 26 (2), 381–394.
Macko, S.A., Estep, M.L.F., 1984. Microbial alteration of stable nitrogen and carbon isotopic compositions or organic matter. Org. Geochem. 6, 787–790.
Martin, L., Suguio, K., Flexor, J.M., 1993. As flutuações do nível do mar durante oQuaternario superior e a evolução de "deltas" brasileiros. Boletim IG-USP 15, 1e186.
Martinez, P., Lopes-Mazzeto, J.M., Buurman, P., Giannini, P.C.F., Schellekens, J., Vidal-Torrado, P., 2018. Geomorphological control on podzolisation – an example from a tropical barrier island. Geomorphology 309, 89–97.
Mckeague, J.A., Wang, C., 1980. Micromorphology and energy dispersive analysis of orstein horizons of podzolic soils from New Brunswick and Nova Scotia, Canada. Can. J. Soil Sci. 60, 9–21 1980.
Mckeague, J.A., Day, J.H., 1966. Dithionite-and oxalate-extractable Fe and Al as aids in differentiating various classes of soils. Can. J. Soil Sci. 1 (1), 13–22.
Mehra, O.P., Jackson, M.L., 1960. Iron oxide removal from soils and clays by a dithionite-citrate system buffered with sodium bicarbonate. Clay Clay Miner. 7 (2), 317–327.
Mendonça, B.A.F., Fernandes Filho, E.I., Schaefer, C.E.G.R., Simas, F.N.B., de Paula, M.D., 2015. Os solos das Campinaranas na Amazônia brasileira: ecossistemas arenícolas oligotróficos. Ciência Florestal, Santa Maria 25 (4), 827–839.
Ministério do Meio Ambiente, 2000. Avaliação e Açoes Prioritárias para a Conservação da Biodiversidade da Mata Atlântica e Campos Sulinos. MMA/SBF, Brasília, pp. 40.
Montes, C.R., Lucas, Y., Pereira, O.J.R., Achard, R., Grimaldi, M., Melfi, A.J., 2011. Deep plant-derived carbon storage in Amazonian podzols. Biogeosciences 8, 113–120.

Moreau, A.M.S.S., Ker, J.C., Costa, L.M., Gomes, F.H., 2006. Caracterização de solos de duas topossequências em Tabuleiros Costeiros do sul da Bahia. Rev. Bras. Ciência do Solo 30 (4), 1007–1019.

Mokma, D.L., Schaetzl, R.J., Doolittle, J.A., Johnson, E.P., 1990. Groundpenetrating radar study of ortstein continuity in some Michigan Haplaquods. Soil Sci. Soc. Am. J. 54, 936–938.

Oliveira, A.P., Ker, J.C., Silva, I.R., Fontes, M.P.F., de Oliveira, A.P., Neves, A.T.G.R., 2010. Spodosols pedogenesis under Barreiras formation and sandbank environments in the south of Bahia. Rev. Bras. Ciência do Solo 34 (3), 847–860.

Perrin, R.M.S., Willis, E.H., Hodge, C.A.H., 1964. Dating of humus podzols by residual radiocarbon activity. Nature 202 (4928), 165–166.

Pessenda, L.C.R., Valencia, E.P.E., Camargo, P.B., Telles, E.C.C., Martinelli, L.A., Cerri, C.C., Aravena, R., Rozanskj, K., 1996. Natural radiocarbon measurements in Brazilian soils developed on basic rocks. Radiocarbon 38 (2), 203–208.

Pessenda, L.C.R., Buso Junior, A.A., Cohen, M.C.L., Calegari, M.R., Schiavo, J.A., França, M., Lorente, F.L., Giannini, P.C.F., Oliveira, P.E., Rossetti, D.F., Siqueira, G.S., Francisquini, M.I., Volkmer-Ribeiro, C., Bendassolli, J.A., Madella, M., Osterrieth, M., Cechet, F.A., Felipe, P.L.L., Brustolin, L.T., Rasbold, G.G., Monteiro, M.R., 2015. Estudos interdisciplinares da dinâmica da vegetação e marinha e inferências climáticas milenares e atuais na costa Norte do Espírito Santo. Ciência & Ambiente 49 (1), 181–206.

Pessenda, L.C.R., De Oliveira, P.E., Mofatto, M., Medeiros, V.B., Garcia, R.J.F., Aravena, R., Bendassoli, J.A., Leite, A.Z., Saad, A.R., Etchebehere, M.L., 2009. The evolution of atropical rainforest/grassland mosaic in southeastern Brazil since 28,000 14C yr BP based on carbon isotopes and pollen records. Quat. Res. 71, 437–452.

Santos, H.G., Jacomine, P.K.T., Anjos, L.H.C., Oliveira, V.A., Lumbreras, J.F., Coelho, M.R., Almeida, J.A., Araújo Filho, J.C., Oliveira, J.B., Cunha, T.J.F., 2018. Sistema Brasileiro de Classificação de Solos. 5a ed. revisada e ampliada. Brasília, DF: Embrapa. pp. 531.

Santos, R.D., Santos, H.G., Ker, J.C., Anjos, L.H.C., Shimizu, S.H., 2015. Manual de descrição e coleta de solo no campo. 7. In: Viçosa, M.G. (Ed.), Sociedade Brasileira de Ciência do Solo/Embrapa Solos, pp. 100.

Saporetti-Junior, A.W., Schaefer, C.E.R., Souza, A.L., Soares, M.P., Araújo, D.S.D., Meira-Neto, J.A.A., 2012. Influence of soil physical properties on plants of the mussununga ecosystem, Brazil. Folia Geobot. 47, 29–39.

Sauer, D., Sponagel, H., Sommer, M., Giani, L., Jahn, R., Stahr, K., 2007. Podzol: soil of the year 2007. A review on its genesis, occurrence, and functions. J. Plant Nutr. Soil Sci. 170 (5), 581–597. https://doi.org/10.1002/jpln.200700135.

Schiavo, J.A., Dias Neto, A.H., Pereira, M.G., Rosset, J.S., Secretti, M.L., Pessenda, L.C., 2012. Characterization and classification of soils in the Taquari river basin - Pantanal region, state of Mato Grosso do sul, Brazil. Rev. Bras. Ciência do Solo 36 (3), 697–707.

Schwartz, D., 1988. Some podzols on Bateke sands and their origins, People's Republic of Congo. Geoderma 43, 229–247.

Sierra, C.A., Jiménez, E.M., Reu, B., Peñuela, M.C., Thuille, A., Quesada, C.A., 2013. Low vertical transfer rates of carbono inferred from radiocarbon analysis in na Amazon Podzol. Biogeosciences 10 (1), 3455–3464.

Silva, E.A., Gomes, J.B.V., Araújo Filho, J.C., Silva, C.A., de Carvalho, S.A., Curi, N., 2013. Podzolização em solos de áreas de depressão de topo dos tabuleiros costeiros do Nordeste Brasileiro. Rev. Bras. Ciência do Solo 37 (1), 11–24.

Stoops, G., 2003. Guidelines for Analysis and Description of Soil and Regolith Thin Sections. Soil Science Society of America, Madison, Wisconsin.

Stuiver, M., Reimer, P.J., 1993. Extended 14C database and revised CALIB 3.0 14C calibration program. Radiocarbon 35 (1), 215–230.

Teixeira, P.C., Donagemma, G.K., Fontana, A., Teixeira, W.G., 2017. Manual de métodos de análise de solo. Rio de Janeiro, 3a ed. Revisada e ampliada – Brasília, DF: Embrapa. pp. 573.

Ucha, J.M., Vilas Boas, G.S., Hadlich, G.M., 2010. O uso do radar de penetração no solo na investigação dos processos de transformação pedogeomorfológica. Revista Brasileira de Geomorfologia 11 (1), 85–96.

Van Breemen, N.V., Buurman, P., 1998. Soil Formation. Kluwer, Dordrecht.

Veríssimo, N., Safford, H.D.F., Behling, H., 2012. Holocene vegetation and fire history of the Serra do Caparaó, SE Brazil. Holocene 22 (11), 1243–1250.

Yeomans, J.C., Bremner, J.M., 1988. A rapid and precise method for routine determination of organic carbon in soils. Commun. Soil Sci. Plant Anal. 19 (4), 1467–1476.